ANL/CP--72768

DE91 010593

HIGH RESOLUTION ELECTRON MICROSCOPY OF GRAIN BOUNDARIES*

K.L. Merkle and Y. Gao

Materials Science Division
Argonne National Laboratory, Argonne, IL 60439

MARCH 1991

---

*Work supported by the U.S. Department of Energy, BES-Materials Sciences, under Contract No. W-31-109-Eng-38.

INVITED manuscript submitted to the Microbeam Analysis Society 25th Annual Meeting, San Jose, California, August 4-9, 1991.

HIGH RESOLUTION ELECTRON MICROSCOPY OF GRAIN BOUNDARIES*

K. L. Merkle and Y. Gao

High-resolution electron microscopy (HREM) has made considerable contributions to our understanding of grain boundaries (GBs) during the past several years, largely stimulated by the availability of instruments with spatial resolution of better than 0.2 nm. We review here some of the results of our HREM investigations on GBs in ceramic oxides, metals and high-temperature superconductors. The emphasis of this paper will be on (a) common features of GBs in different materials, (b) quantification of atomic scale structures in large-angle GBs, and (c) investigation of interrelationships between atomic structure and properties of GBs.

Grain Boundary Geometry

Irrespective of the crystal structure of the grains, the macroscopic characterization of a grain boundary involves five macroscopic and three microscopic degrees of freedom. This large multitude of possible arrangements of the interface makes it an extremely complex task to relate GB properties to GB structure.

The macroscopic geometry of a GB is usually described in terms of a bicrystal, where one crystal is rotated relative to the other via a misorientation (axis and angle) and a plane, which defines the boundary within this bicrystal. A special subset of possible bicrystals is given by the notionally interpenetrating lattices that form a coincident site lattice (CSL) with the reciprocal density of coincident sites Σ.[1]

An alternative description [2] uses the crystallographic planes $(h\ k\ l)_1$ and $(h\ k\ l)_2$ that are joined at the interface and a rotation ψ around the GB normal $\hat{n}$ to define the macroscopic GB

---

* The authors are with the Interface Studies Group, Materials Science Division, Argonne, National Laboratory, Argonne, IL 60439. This work was supported by the U.S. Department of Energy, Basic Energy Sciences, under contract W-31-109-Eng-38 and the National Science Foundation--Office of Science and Technology Centers under contract #STC-8809854 (Y. G.).

geometry. For a general θ the GB contains twist and tilt components, but for both of the special rotations $\psi = 0°$ and $\psi = 180°$, asymmetric *tilt* GBs are formed whenever $(h\ k\ l)_1 \neq (h\ k\ l)_2$, otherwise, i. e. for $(h\ k\ l)_1 = (h\ k\ l)_2$, $\psi = 0°$ and $\psi = 180°$ represent the ideal lattice and *symmetric* tilt GBs, respectively. Recent computer simulations of GBs in fcc and bcc metals have indicated that the GB energy as a function of ψ shows deep cusps at $\psi = 0°$ and $\psi = 180°$[3,4]. Therefore, tilt GBs are distinguished from all other configurations by their low energy. It is a favorable circumstance that those same boundaries, provided their tilt axis coincides with a low index zone axis, are readily accessible to HREM observation.

The GB *energy* is the most important factor in determining the types of GB geometries that are naturally occurring in polycrystals and is also thought to play a central role in various GB properties, for example, in impurity segregation, fracture, and GB diffusion. Exploration of the connection between GB energy and structural parameters, such as macroscopic geometry, atomic-level geometry (rigid-body translations), and the detailed nature of the atomic relaxations at the GB core and near the GB, are therefore a prime goal of GB research. In the following we report results from HREM investigations of the fcc model systems NiO and Au in which the atomic structures have been explored for a range of macroscopic GB parameters. HREM investigations can also illuminate the connections between GB geometry, atomic-scale structure and supercurrent transport properties in $YBa_2Cu_3O_{7-x}$.

The Role of the Grain Boundary Plane

Bicrystal experiments are particularly well suited for studies of the role of the GB plane in GB structure and energy. Fig. 1 shows a TEM image of a $<1\bar{1}0>$ tilt GB in Au (near Σ=9). The strong faceting of the GB into planar facets clearly indicates that some GB inclinations are preferred over others. However, atomic-scale resolution is needed to identify the facet planes and GB core structures. For example, the most prominent facets in Fig. 1 are of the (111)(551) type, for which the GB decomposes into triangular regions bounded by two (111)(111) and one (112)(112) GB. A single unit of this type from another $\Sigma = 9$ bicrystal is shown in Fig. 2. This dissociated GB is attached to a symmetric and an asymmetric GB on the

left and right in Fig. 2, respectively. The occurrence of asymmetric GBs, where at least one of the GB planes is dense-packed (i. e. a low-index plane) is a common feature of many large-angle GBs, also in NiO (Fig. 3). This indicates that such boundaries may be low in energy.[5-8] Indeed, recent HREM studies in combination with computer simulation of Σ=9 and Σ=11 GBs in Au have shown that the facet formation agrees with GB energy calculations (including the dissociation of the (111)(115)GB) and that asymmetric GBs often have lower energies than the corresponding symmetric facets.[9, 10]

On any given plane, the GB core structure is not necessarily unique, as illustrated in Fig. 4, which shows two variants of the (310)(310) tilt GB in NiO.[11] In atomistic computer simulations of GBs one frequently finds GB structures that have similar energies for the same macroscopic GB parameters.[12] Multiple GB structures have recently been found by HREM in a number of materials.[13-15]

Another aspect of the role of the GB plane concerns the uniqueness of the structural repeat units. When, for example two low-index planes are joined together to form a GB, the atomic repeat distances would typically be incommensurate, at least in one direction along the plane of the GB. Therefore, no unique structural unit can be defined which would generate the atomic structure of the interface by periodic continuation. In contrast to computer simulation, which is largely limited to the investigation of periodic models of GBs, HREM can study the real structure of interfaces, including aperiodic features and structural defects. An interesting case in point is the (111)(001) GB, at the $<1\bar{1}0>$, $\theta = 54.73°$ misorientation, which is very close to the $\Sigma = 41$, $\theta = 55.88$ misorientation. In Figure 5 regions of good atomic match alternate with localized regions of misfit that are accompanied by lattice strain at rather short repeat distances. This boundary is quasiperiodic and represents the GB analogue to the formation of misfit dislocations in heterophase boundaries.[16] Similar to Au, quasiperiodic boundaries have also been observed in NiO (see Fig. 6).[6]

Atomic Matching

Low-angle GBs have long been known to provide smooth transitions between the two lattices on either side of the GB by accommodating the misfit in spatially localized regions in the form of primary edge- or screw dislocation. Misfit localization also plays an important role in large-angle GBs, as first suggested by Mott.[17] An example for misfit localization observed by HREM in a large-angle GB was given in Fig. 5. The localizations of misfit can take various forms, such as misfit-dislocation-like defects in quasiperiodic boundaries (see Fig. 5), three-dimensional structures,[16] and localization of misfit within large structural units of GBs with large planar unit cells. Common features of all GBs are (a) the tendency of the atoms within the GB to assume positions which , as much as possible resemble the local environment in the ideal lattice and (b) that the atomic relaxations are rather local in large-angle GBs. Therefore a boundary, such as the $\Sigma = 41$ (near (111)(001), Fig. 5) with a rather long structural period, seeks out its minimum energy state more as a result of local atomic relaxations rather than by preserving its long-range structural periodicity. Atomically well-matched structures can often be recognized in HREM by an apparent elastic continuation of low-index planes across the GB.[18]

Quantification of atomic-scale GB parameters

The rigid-body displacements between the two halves of a bicrystal have been recognized since the earliest GB computer simulations to provide an important relaxation mechanism for the minimization of the GB energy.[19] Following this, several EM methods have been developed to measure this important quantity.[20-24] Most of these methods are quite limited in their applicability (with the exception of the Fresnel technique,[24, 25] which is complementary to the HREM method) and only the HREM technique allows the identification of the GB core structure, which is important for the derivation of absolute values of the rigid-body translation normal to the interface.[26] We have expanded the HREM technique used by Stobbs and co-workers [23, 27] (see Fig. 8) to also allow highly accurate measurements of the volume expansion δ (i. e. the component normal to the GB) when the GB is not parallel to major

crystallographic planes on either side of the interface.[28] Recent computer simulation results for a large range of high-angle GB geometries have revealed an approximately linear relationship between GB energy and the volume expansion.[3,4] With the exception of the coherent twin (111)(111), which has practically zero volume expansion, measured values of δ for Au are a factor of two or more higher than the calculated values, based on embedded-atom-method (EAM) potentials.[15,29] The origin of this discrepancy between experimental and calculated volume expansions in Au is not known at present. In contrast to Au, the volume expansion of the $\Sigma = 5$, (310) GB in NiO has been found to be considerably smaller than calculated.[11]

A quantification of the unavoidable atomic disorder at a GB can be attempted by considering the local atomic environment of each atom in the GB. Wolf has recently discussed the correlation between GB energy and the number of "broken bonds" per unit GB area [3,30]. Although the HREM technique gives at best a two-dimensional projection of the atomic structure and therefore requires observations along more than one zone axis for a three-dimensional reconstruction of a GB, one can attempt to construct three-dimensional models of tilt GBs based on the assumption that there are no shifts along the direction of observation. Using this simple model, we have analyzed HREM images such as in Fig. 9, in terms of the number of "broken bonds" per GB unit area.

By determining the number of atoms within a shell that bisects the distance between first and second nearest neighbors in the ideal lattice, the number of "broken bonds" can be found for each atom n within the GB structural unit as the deviation $\Delta K_n = K_n - K_{id}$ from the perfect fcc crystal coordination number, $K_{id}=12$. Following Wolf ,[3,30] the coordination coefficient $C = 1/A \sum_n | K_n - K_{id}|$, i. e. the number of "broken bonds" per GB unit area A is found by summing over all atoms in the GB unit cell. The number of "broken bonds" per GB unit area is plotted in fig. 10 for several symmetric $<1\bar{1}0>$ tilt GBs in Au and shows a close to linear relationship to the calculated EAM energies for these boundaries.

Grain Boundary Structure and Properties

So far we have considered various aspects of the atomic structure of simple fcc GBs and their connection to GB energy. We shall now give two examples of HREM investigations of GBs in the orthorhombic high-Tc superconductor $YBa_2Cu_3O_{7-x}$. Here the atomic structure and chemical composition of the interface is related to the capacity for carrying electric current across the interface.

For <001> tilt GBs in $YBa_2Cu_3O_{7-x}$ Dimos et al.[31] found that the critical current density across the GBs decreases by more than an order of magnitude as the misorientation angle θ increases from 0 to 11° and stays relatively constant at angles greater than 15°. We have observed small-angle GBs of the same geometry in MOCVD-grown $YBa_2Cu_3O_{7-x}$. As expected, the GBs consist of a set of appropriately spaced edge dislocations (Burgers vector a[100]). The lattices were smoothly connected between the two crystals in the GB regions separating the discrete dislocations. One dislocation core, observed by HREM is shown in Fig. 11a. Strong atomic relaxations are present, but the most striking feature is that the core region has a finite size, 2 nm in diameter. Image simulations based on a model which maintains the chemical composition of the lattice at the GB core (Fig. 11c) cannot reproduce the observed image. However, when the Y-Ba columns are replaced by Cu columns, one obtains a good match between observed and simulated images (Fig. 11d). To confirm this model, efforts will be undertaken to directly measure the composition of individual dislocation cores by analytical techniques.

Our HREM analysis suggests that the dislocation cores are not superconducting. In a dislocation model of the GB, the cores would start to overlap at 11°, given the observed size of the dislocation cores. Thus the rapid decrease of the critical current as a function of tilt angle observed by Dimos et al. could be explained by our observations.[32]

A large-angle $YBa_2Cu_3O_{7-x}$ GB of considerable interest is shown in Fig. 12. The misorientation for this GB is characterized by a <100> tilt axis and a misorientation angle of 90°. Thus (001)(010) boundaries (horizontal section in Fig. 12) can be formed. The

superconducting transport properties of bicrystal specimens with the same macroscopic configuration have recently been investigated by Babcock et al. and their results suggested weak-link-free behavior for these GBs.[33] We have investigated the atomic structure of the (001)(010) GB in detail by comparisons between simulated images and the observation.[34] Two possible atomic models, both of which represent very well-matched structures that maintain the structural integrity of the superconducting phase at the interface, are consistent with the HREM images.

In spite of the atomically well-matched (001)(010) interface which maintains complete $YBa_2Cu_3O_{7-x}$ unit cells at the GB, the direct coupling of the supercurrent across the interface should be limited to Cu-O planes immediately adjoining the GB. However, at the <100>, θ = 90° misorientation we also find symmetric (013)(013) facets (see Fig. 12). The latter provide a direct connection between the Cu-O planes, thus suggesting the possibility of strong supercurrent coupling across this large-angle interface.[34]

Summary and Conclusions

Systematic HREM investigations have provided new insights into the atomic structure of GBs. The application of this atomic-scale information to the understanding of GB properties may in the future allow for the possibility of prediction and modification of GB properties.

HREM studies of a number of GBs in NiO and Au have clearly demonstrated that a general tendency exists to produce atomically well-matched structures and to preserve a high degree of coherency across the interface. HREM observations have established that misfit-dislocation-like defects are formed in large-misfit, incommensurate grain boundaries. We expect that these and other general structural features that have been investigated in NiO and Au are typical for other ceramic and metal GBs.

Considerable progress has been made regarding the quantification of structural GB parameters via HREM. Whereas several discrepancies between observed and calculated GB parameters remain, it is expected that the mutual feedback between HREM observations and GB computer simulation will serve as a stimulus to improve both the experimental and

theoretical techniques and will lead to a better understanding of the complicated interrelations between GB structure and properties.

Atomic structure information obtained from HREM observations on $YBa_2Cu_3O_{7-x}$ GBs has led to a much improved understanding of the critical current behavior in these systems.

Direct correlations between atomic structure, including chemical composition, and property measurements on individual GBs will be important for a full understanding of many grain boundary properties.

References

1. W. Bollmann, Crystal defects and crystalline interfaces, Berlin: Springer, 1970.
2. D. Wolf and J. F. Lutsko, "On the geometrical relationship between tilt and twist grain boundaries" Zs. f. Kristall. 189: 239, 1989.
3. D. Wolf, "Structure-energy correlation for grain boundaries in fcc metals - III. Symmetrical tilt boundaries" Acta Metall. Mater. 38: 781, 1990.
4. D. Wolf, "Structure-energy correlation for grain boundaries in fcc metals - IV. Asymmetrical twist (general) boundaries" Acta Metall. Mater. 38: 791, 1990.
5. D. Wolf, "On the relationship between symmetrical tilt,twist,"special", and "favored" grain boundaries" J. de Physique 46: 197, 1985.
6. K. L. Merkle and D. J. Smith, "Atomic resolution electron microscopy of NiO grain boundaries" Ultramicroscopy 22: 57, 1987.
7. K. L. Merkle, J. F. Reddy, C. L. Wiley, and D. J. Smith, "Structure of High-angle grain boundaries in NiO" in J. A. Pask and A. G. Evans, Eds., Ceramic Microstructures '86, Role of Interfaces, 1987, 241.
8. D. Wolf, "Comparisons of the Energies of symmetrical and asymmetrical grain boundaries" in J. A. Pask and A. G. Evans, Eds., Ceramic Microstructures '86, Role of Interfaces, 1987, 177.
9. K. L. Merkle and D. Wolf, "Structure and Energy of grain boundaries in metals" MRS Bulletin 15: 42, 1990.

10. K. L. Merkle and D. Wolf, "Low-energy configurations of symmetric and asymmetric tilt grain boundaries" submitted to Phil. Mag. 1990.

11. K. L. Merkle and D. J. Smith, "Atomic Structure of symmetric tilt grain boundaries in NiO" Phys. Rev. Lett. 59: 2887, 1987.

12. V. Vitek, A. P. Sutton, G. J. Wang, and D. Schwartz, "On the Multiplicity of Structures of grain boundaries" Scripta Met. 17: 183, 1983.

13. J. L. Rouvière and A. Bourret, "Multiple Structures of a <001> Σ=13 tilt grain boundary in Ge." in Polycrystalline Semiconductors, Springer Proceedings in Physics **35**, Berlin: Springer-Verlag, 1988, 19 .

14. M. J. Mills and M. S. Daw, "The study of defects in metals using HRTEM and atomistic calculations" Mat. Res. Symp. Proc. 183: 15, 1990.

15. K. L. Merkle, "High-resolution Electron Microscopy of grain boundaries in fcc Materials" Colloque de Phys. 51 C1-: 251, 1990.

16. K. L. Merkle, "Quasiperiodic interfaces: HREM observations of grain and phase boundaries" in Electron Microscopy 1990, L. D. Peachy and D. B. Williams Eds., **4**, San Francisco Press, 1990) p. 332 .

17. N. F. Mott, "Slip at grain boundaries and grain growth in metals" Proc. Phys. Soc. 60: 391, 1948.

18. K. L. Merkle, "Atomic matching across internal interfaces" Mat. Res. Soc. Symp. Proc. 153: 83, 1989.

19. M. J. Weins, H. Gleiter, and B. Chalmers, "Computer calculations of the structure of high-angle grain boundaries" J. Appl. Phys. 42: 2639, 1971.

20. R. C. Pond and D. A. Smith, "An experimental technique for detecting rigid-body translations between adjacent grains" Can. Metall. Quarterly 13: 39, 1974.

21. J. W. Matthews and W. M. Stobbs, "Measurement of the lattice displacement across a coincidence grain boundary" Phil. Mag. 36: 373, 1977.

22. R. C. Ecob and W. M. Stobbs, "The use of moire techniques to measure rigid-body displacements" J. Microsc. 129: 275, 1983.

23. W. M. Stobbs, G. J. Wood, and D. J. Smith, "The measurement of boundary displacements in metals" Ultramicroscopy 14: 145, 1984.

24. C. B. Boothroyd, A. P. Crawley, and W. M. Stobbs, "The measurement of rigid-body displacements using Fresnel fringe intensity methods" Phil. Mag. A 54: 663, 1986.

25. W. M. Stobbs, "The TEM of interfaces and multilayers" in Surface and Interface Characterization by Electron Optical Methods, A. Howie and U. Valdrè Eds., NATO ASI Series B 191, Plenum Press, 1988, 77 .

26. K. L. Merkle, "Rigid-body displacement of asymmetric grain boundaries" Scripta Met. 23: 1487, 1989.

27. G. J. Wood, W. M. Stobbs, and D. J. Smith, "Methods for the measurement of rigid-body displacements at edge-on boundaries using HREM" Phil. Mag. A 50: 375, 1984.

28. K. L. Merkle, in Proceedings of the Worshop on Structure and Properties of Interfaces, Wickenburg, submitted to Ultramicroscopy (1991).

29. F. Cosandey, S.-W. Chan, and P. Stadelmann, "HREM Studies of [001] tilt grain boundaries in Gold" Colloque de Phys. 51: C1-109, 1990.

30. D. Wolf, "A broken-bond model for grain boundaries in fcc metals" J. Appl. Phys. 68: 3221, 1990.

31. D. Dimos, P. Chaudhari, J. Mannhart, and F. K. LeGoues, "Orientation dependence of grain boundary critical currents in $YBa_2Cu_3O_{7-x}$ bicrystals" Phys. Rev. Lett. 61: 219, 1988.

32. Y. Gao, K. L. Merkle, G. Bai, H. L. M. Chang, and D. J. Lam, "Structure and composition of grain boundary dislocation cores and stacking faults in MOCVD-grown $YBa_2Cu_3O_{7-x}$ thin films" Physica C 174: 1, 1991.

33. S. E. Babcock, X. Y. Cai, D. L. Kaiser, and D. C. Larabalestier, "Weak-link-free behaviour of high-angle $YBa_2Cu_3O_{7-x}$ grain boundaries in high magnetic fields" Nature 347: 167, 1990.

34. Y. Gao, G. Bai, D. J. Lam, and K. L. Merkle, "Microstructure and defects in a-axis oriented $YBa_2Cu_3O_{7-x}$ thin films" Physica C 173: 487, 1991.

35. D. Wolf , private communication, 1991.

Figure captions

Fig. 1. Transmission electron micrograph of <1$\bar{1}$0> tilt GB in Au. Coexistence of extended planar symmetric (S) with a number of asymmetric facets is evident.

Fig. 2. Axial HREM image (white atomic columns) of <110> tilt bicrystal in Au, viewed along <110> tilt axis. Misorientation $\theta = 39°$ (Σ=9). The GB translates from the (114)(114) GB at the top to the dissociated (111)(115), and to the (11,11,1)(111) at the bottom.

Fig. 3. NiO <001> $\Sigma = 5$ bicrystal (black atoms) with horizontal, asymmetric (430)(100) facet that translates to symmetric (210)(210) GB on the right.

Fig. 4. A small step separates the two variants of the (310)(310) GB in NiO (black atoms).

Fig. 5. (111)(001), <1$\bar{1}$0> tilt GB in Au ($\theta = 55°$). This GB is quasiperiodic and shows misfit localization in the form of misfit-dislocation-like defects.

Fig. 6. Incommensurate (210)(100) <001> tilt GB in NiO (black atoms). grain boundaries often incorporate relatively dense-packed planes.

Fig. 7. Atomically well-matched large-angle <1$\bar{1}$0> symmetric tilt GB in Au (white atoms). (443)(443), $\theta = 55°$. Note misfit localization and relaxation of (111) planes in compressed image (bottom).

Fig. 8. Analysis of volume expansion is based on digitized images and extrapolation of column positions from outside of the range of elastic distortions associated with the GB.

Fig. 9. GB structural unit of the (443)(443), <1$\bar{1}$0> tilt GB in Au. Atom positions within the repeat unit are identified by circles. Small and large circles indicate the assignment used for A and B layers, respectively.

Fig. 10. Coordination coefficient ("broken bonds" per unit GB area) vs. GB energy (from EAM calculations [35]). Note the practically linear relationship between miscoordination and GB energy.

Fig. 11. (a) HREM image of a dislocation core in low-angle <001> tilt GB of $YBa_2Cu_3O_{7-x}$. (b) Atomic structure of the dislocation core based on the positions of atomic columns in (a). The full and open circles represent the Cu-O and Y-Ba columns in the <001> direction, respectively. (c) Simulated image where the atomic columns at the core, marked by $\oplus$ in (b), are, as in the bulk, Y-Ba columns. (d) Simulated image based on the model in which the Y and Ba at the core are replaced by Cu columns. The image in (d) matches closely the HREM image in (a), indicating the material at the core is non-superconducting.

Fig. 12. HREM image of <100>, $\theta = 90°$ tilt GBs in $YBa_2Cu_3O_{7-x}$. Both (010)(001) and (013)(013) GBs are present. The (013)(013) GBs provide a good connection between the Cu-O planes across the GB and are therefore believed to be responsible for the "weak-link-free" behavior.[33]

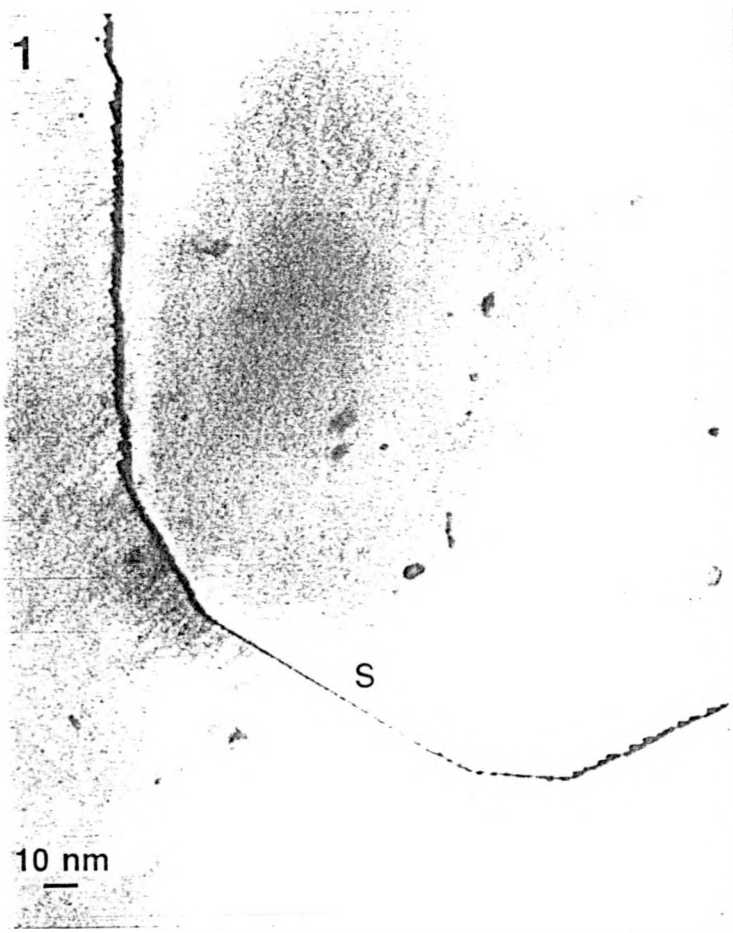
1
S
10 nm

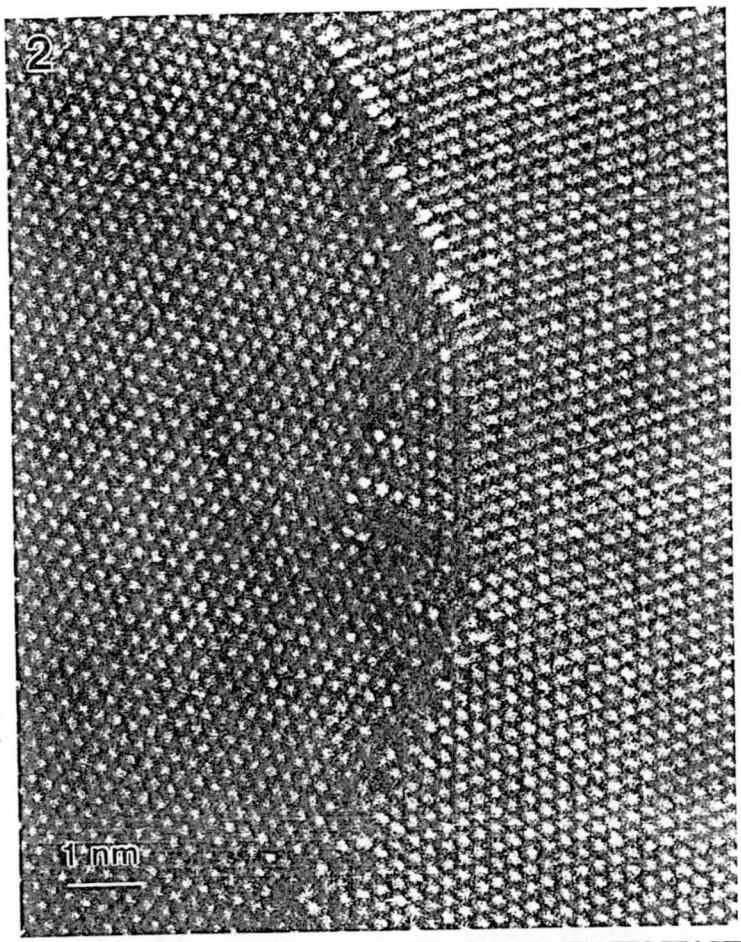
2
1 nm

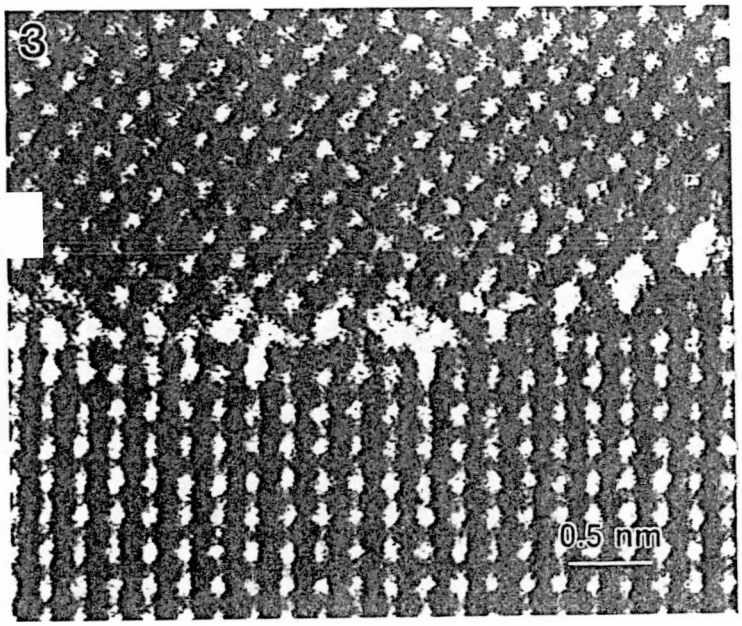
3
0.5 nm

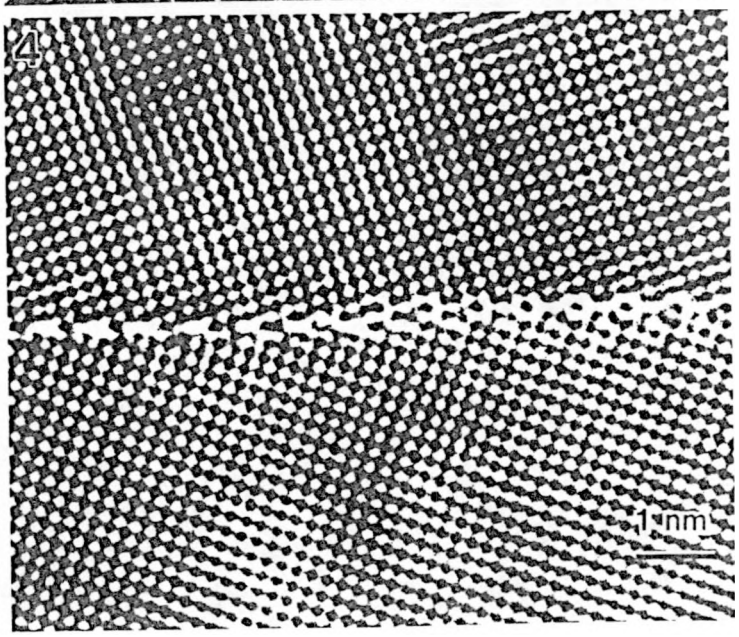
4
1 nm

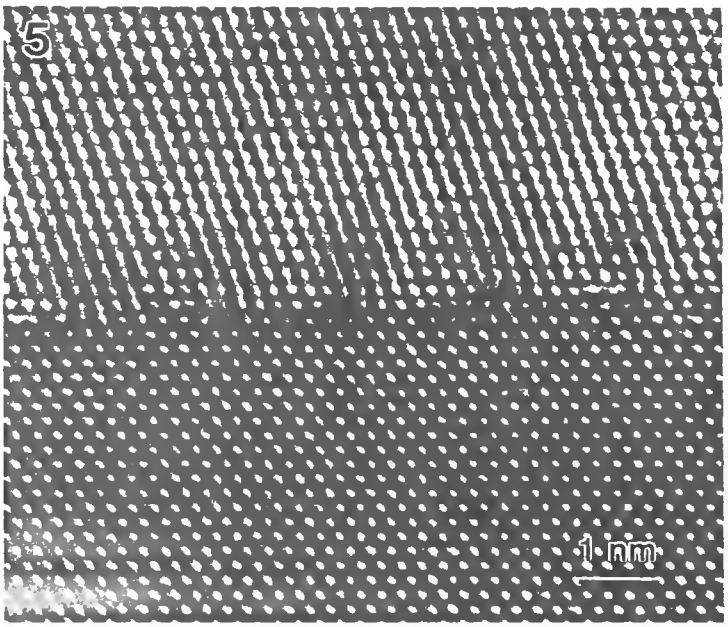
5
1 nm

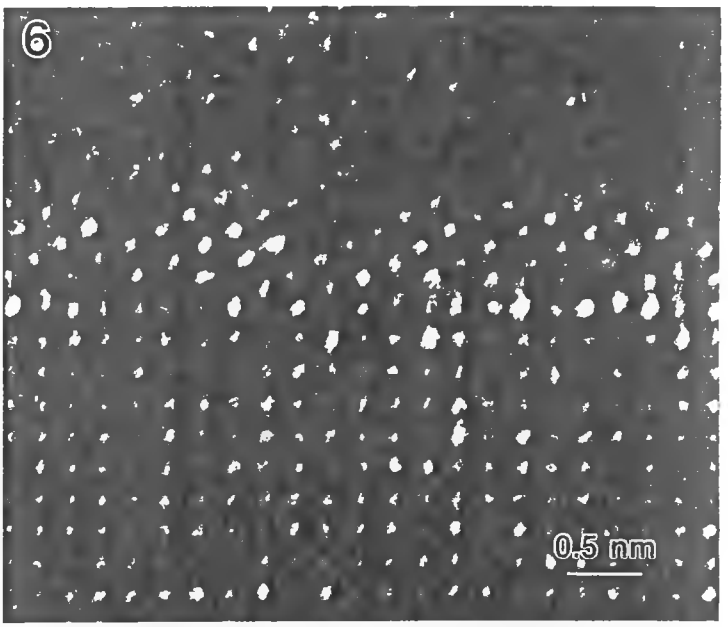
6
0.5 nm

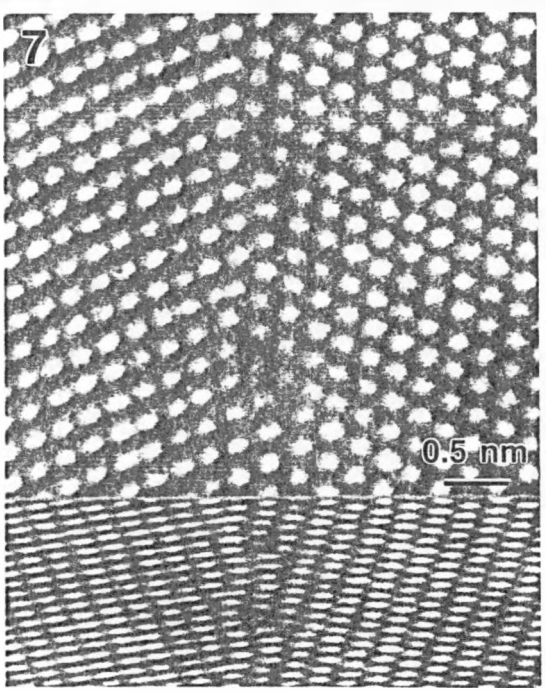
7
0.5 nm

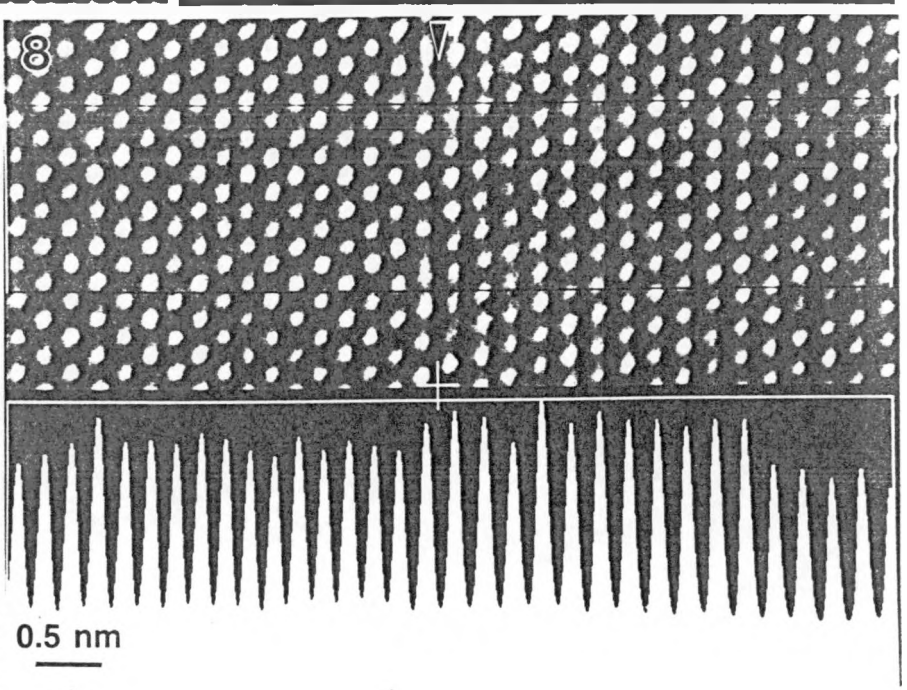
8
0.5 nm

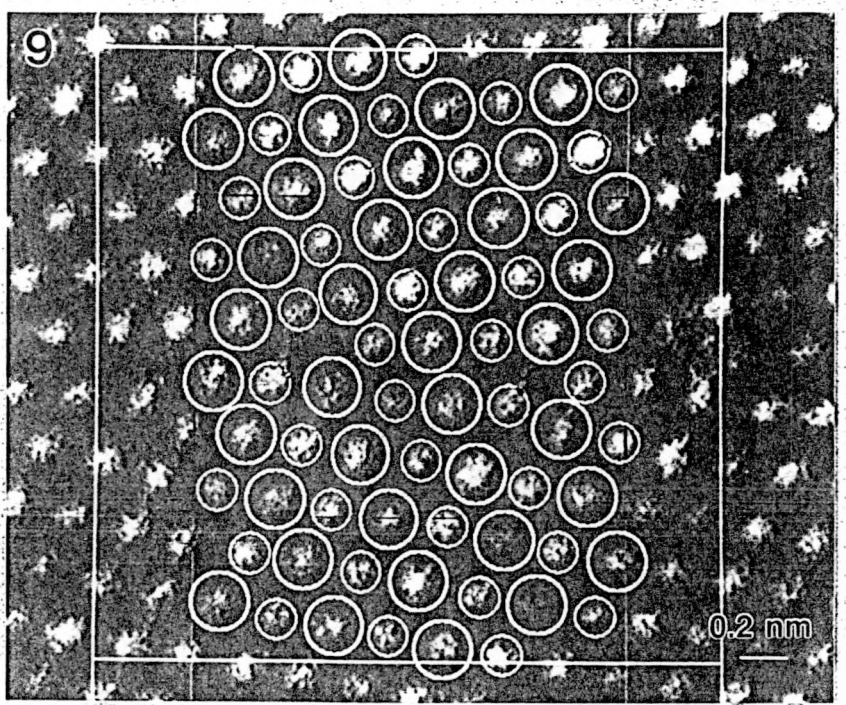
9
0.2 nm

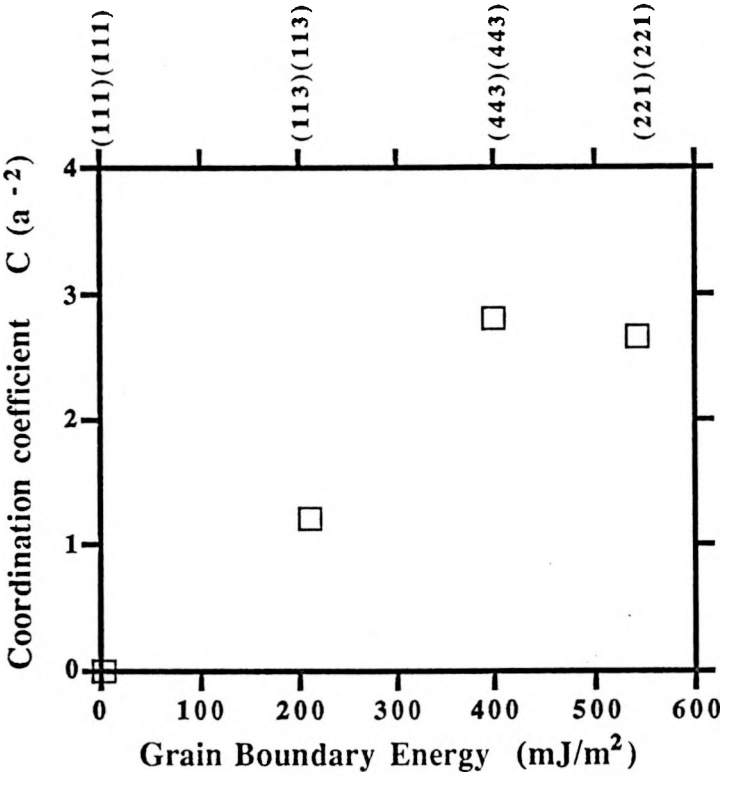

Merkle & Gao
Fig. 10

11

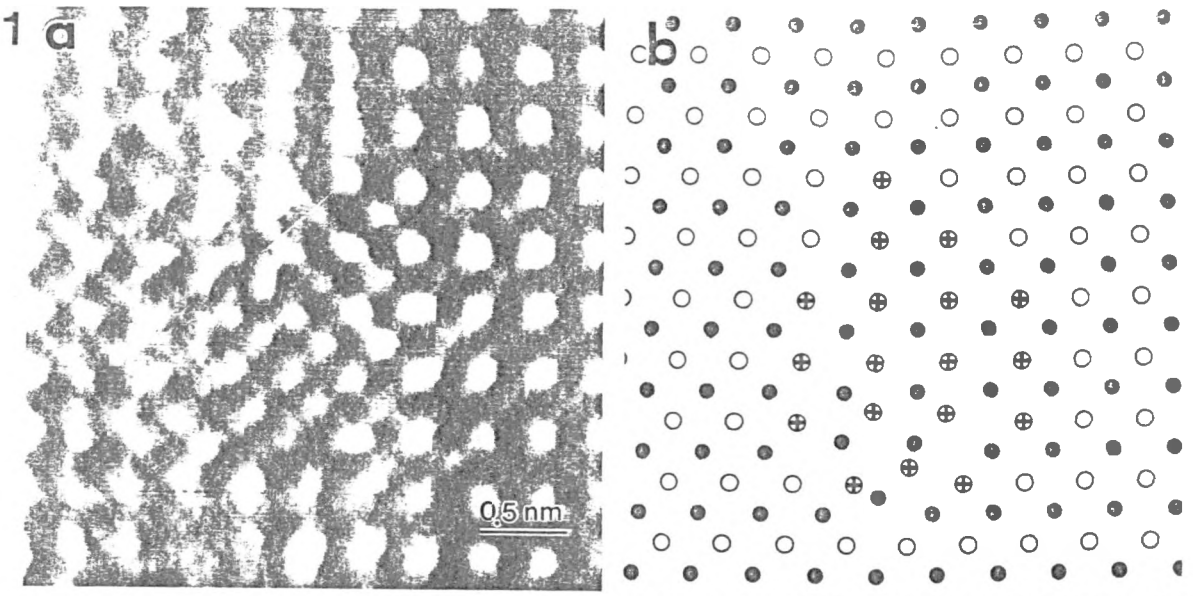

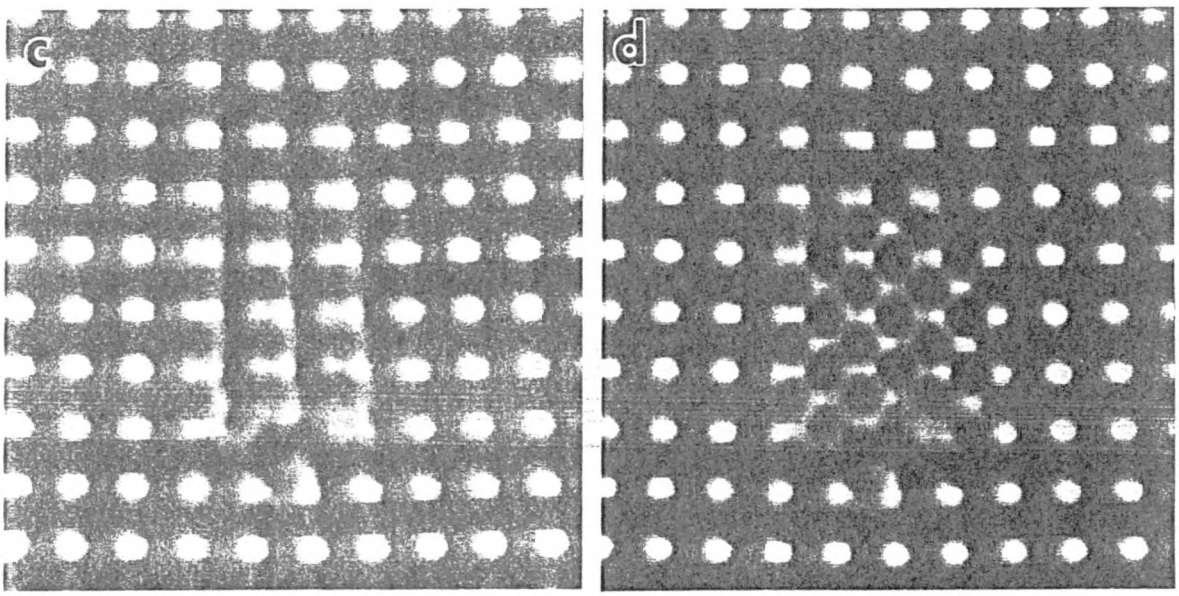

12